Matter

CellPress

Article

Orientation-engineered 2D electronics on van der Waals dielectrics

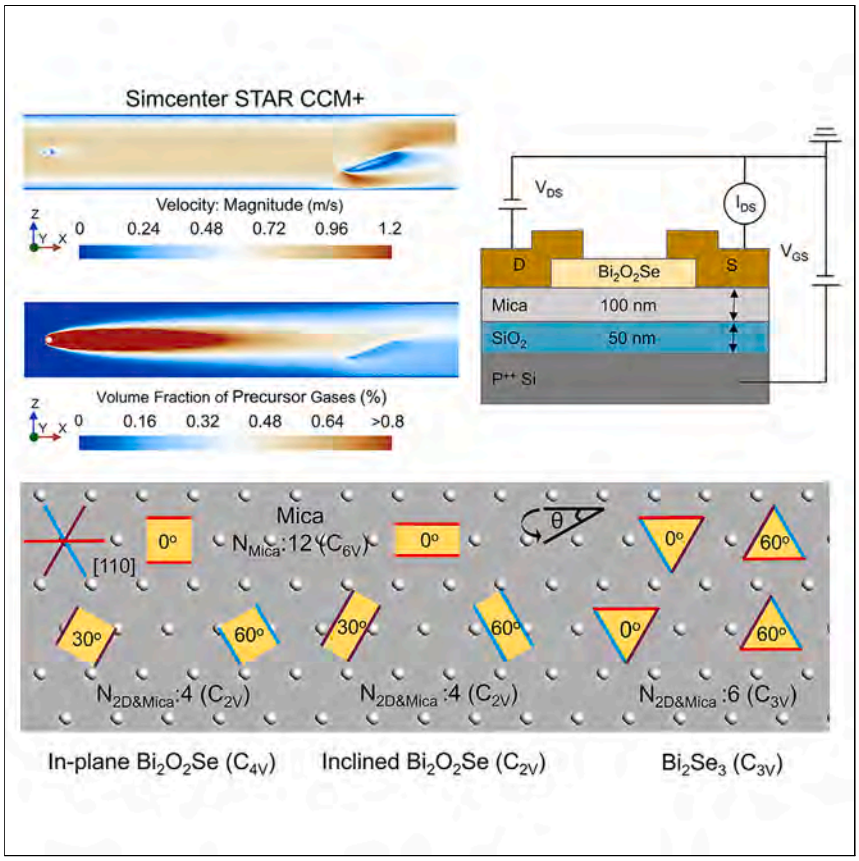

Coordinated with Simcenter STAR CCM+ simulation, a hydromechanical strategy is initiated to achieve the aligned epitaxy of 2D materials on vdWs mica dielectrics. Combining density functional theory with Lagrange's group theorem, a criterion for how the oriented epitaxial growth of the 2D material on a 6-fold symmetric vdWs dielectric is quantitatively established. Moreover, the electrical characteristics of ultrathin as-grown Bi_2O_2Se-based FETs supported on their original epitaxial dielectric are evaluated at the device level.

Weijun Wang, Yuxuan Zhang, Wei Wang, ..., SenPo Yip, Weida Hu, Johnny C. Ho

wdhu@mail.sitp.ac.cn (W.H.)
johnnyho@cityu.edu.hk (J.C.H.)

Highlights

Designed a hydromechanical strategy for aligned 2D material synthesis

Quantitatively established the epitaxy relationship between 2D materials and vdWs dielectrics

Demonstrated high-performance devices with as-grown 2D materials/vdWs dielectrics

Development
Practical, real world, technological considerations and constraints

Wang et al., Matter 7, 2236–2249
June 5, 2024
https://doi.org/10.1016/j.matt.2024.04.013

CellPress

Matter

Article

Orientation-engineered 2D electronics on van der Waals dielectrics

Weijun Wang,[1] Yuxuan Zhang,[1] Wei Wang,[1] Min Luo,[2] You Meng,[1] Bowen Li,[1] Yan Yan,[1] Di Yin,[1] Pengshan Xie,[1] Dengji Li,[1] Dong Chen,[1] Quan Quan,[1] SenPo Yip,[3] Weida Hu,[2,*] and Johnny C. Ho[1,3,4,5,*]

SUMMARY

van der Waals (vdWs) dielectrics are widely used in nanoelectronics to preserve the intrinsic properties of two-dimensional (2D) semiconductors. However, achieving aligned growth of 2D semiconductors and their direct utilization on original vdWs epitaxial dielectrics to avoid disorders poses significant challenges. Here, a hydromechanical strategy for aligned epitaxy of 2D materials on naturally occurring vdWs mica dielectrics is developed. By combining density functional theory with Lagrange's group theorem, a quantitative criterion for 2D material epitaxy on 6-fold symmetric vdWs dielectrics is established. Moreover, the as-grown ultrathin Bi_2O_2Se-channeled field-effect transistor, with a hybrid dielectric layer, achieves a superior current on/off ratio (1.4×10^7) and high carrier mobility ($22.4\ cm^2\ V^{-1}\ S^{-1}$) by directly integrating as-grown 2D materials/vdWs dielectrics. This work provides a powerful methodological platform for aligned 2D material synthesis, alignment direction prediction, and intrinsic property investigation, laying the foundation for advanced electronics on as-grown 2D materials/vdWs dielectrics.

INTRODUCTION

Batch fabrication of advanced two-dimensional (2D) field-effect transistors (FETs) necessitates the synthesis of high-quality 2D films, which is commonly accomplished by aligned coalescence of 2D material islands on specific substrates.[1–3] However, the as-grown 2D films via the mainstream chemical vapor deposition (CVD) method are generally coalesced by enormous misoriented 2D material islands and may be meticulously detached from the original substrates onto proposed dielectrics for further device fabrication.[4,5] Such processes can separately cause grain-boundary-induced disorders and surrounding disorders from chemical adsorbates or neighboring dielectrics, degrading the 2D material's intrinsic properties,[3,6] such as carrier mobility and gate controllability. Compared to the 2D FETs based on conventional oxide dielectrics (such as SiO_2),[7] the devices integrated with van der Waals (vdWs) dielectrics exhibit improved mobility and better switching stability,[8,9] attributable to their atomically flat surfaces that are free of dangling-bond-induced disorders. Thus, achieving aligned growth of 2D materials and directly using them on their original vdWs epitaxial dielectrics to avoid disorders is being pursued with purposefully engineered off-cut angles toward future 2D nanoelectronics.[10,11] Regrettably, achieving non-destructive manipulation of as-grown 2D materials with vdWs dielectrics, e.g., h-BN,[12] Sb_2O_3,[13,14] etc., is currently challenging, hindering the direct integration of as-grown 2D materials on their original vdWs dielectrics.

PROGRESS AND POTENTIAL

Empowered by device miniaturization approaching the physical limits, 2D materials emerge as virtuosos, significantly influencing the trajectory of electronics in the post-Moore era. Leveraged by the hydromechanical strategy, 2D materials with preferential orientations on van der Waals (vdWs) dielectrics can be synthesized, facilitating the direct utilization of as-grown 2D materials/vdWs dielectrics at the device level to minimize disorder-induced performance degradation. Additionally, the establishment of the quantitative criterion for the epitaxy relationship with vdWs dielectrics can be aptly viewed as a measure of our understanding and can guide experimental decisions effectively. This work introduces a powerful methodology platform for synthesizing aligned 2D materials, predicting alignment directions, and preserving their intrinsic properties, holding substantial technological implications for unlocking the transformative potential of 2D materials.

Fortunately, the recent discovery of a naturally occurring vdWs dielectric, muscovite mica, has shed light on exploring those above challenging 2D nanoelectronic issues. Except for the dangling-bond-free surface that facilitates the aligned growth of various 2D materials,[15–18] the mica dielectric provides rich redundancy of being precisely manipulated to desired thicknesses, owing to the relatively weak interlayer interaction.[19] Also, it has a dielectric constant of 6.4–9.3,[20] nearly twice that of the conventional SiO_2 and h-BN, making it applicable for effective gate control and high-speed switching even down to a few atomic layers thick.[3,21] Besides, mica with a large band gap (5.1 eV),[22] high dielectric strength (0.1–1 V/nm),[23] and superior stability can make it an excellent dielectric layer, suitable for high electric fields and high-temperature harsh environments.[24,25] In this regard, relying on vdWs mica dielectrics to develop advanced techniques for achieving aligned synthesis of 2D materials and direct utilization of as-grown 2D materials/vdWs dielectrics are fundamentally feasible and of great significance.

Herein, a hydromechanical strategy for achieving the aligned epitaxy of 2D materials on vdWs mica dielectrics, coordinated with Simcenter STAR CCM+ simulation, is first developed for the promising high-quality synthesis of large-scale 2D films via the coalescence process. In order to gain further insights into the epitaxial relationship between the 2D material and the 6-fold vdWs dielectric, we perform a systematic theoretical analysis by combining the density functional theory (DFT) calculation with Lagrange's group theorem. After that, an unreported criterion for how the epitaxial growth of the 2D material on a 6-fold symmetric vdWs dielectric is established. Moreover, a reproducible technique for high-precision manipulation of as-grown 2D materials on their original vdWs mica dielectric is initiated, while the electrical characteristics of ultrathin as-grown Bi_2O_2Se-based FETs supported on its original vdWs epitaxial substrate are evaluated at the device level.

RESULTS AND DISCUSSION

Aligned fabrication of the 2D materials

Figure 1A depicts a conventional CVD setup with a horizontally positioned growth substrate. As indicated by the carrier gas flow, prolonged precursor transport reduces the control over precursor concentration and growth temperature,[26–28] resulting in non-uniform deposition of various Bi–O–Se products (Figure 1B), including in-plane Bi_2O_2Se, inclined Bi_2O_2Se, and Bi_2Se_3 nanoflakes, respectively. Disordered epitaxial growth on mica is observed for each product (Figure S1), owing to the poor controllability over the precursor transport process and growth temperature. In contrast, as shown in Figure 1C, different compositions can be controllably synthesized by regulating the growth temperature and the precursor weight ratio in the hydromechanics-based CVD system (Note S1), where the growth substrate is inclinedly placed in the CVD system (Figure S2). Figures 1D–1F show the optical microscope images of as-grown 2D products on the titled mica with an angle of around 20°, demonstrating significantly better thickness uniformity and flake orientation in the modified CVD system. Remarkably, the results show that the in-plane and inclined Bi_2O_2Se crystals show three equivalent but different alignment angles on the mica substrate, while only two different orientations are observed for synthesizing 2D Bi_2Se_3 (detailed explanations will be provided later to investigate the intimate interplay between the 2D material and the mica substrate). A series of unique epitaxy characteristics for different 2D products, including orientations and morphology evolution, are observed (Figures S3–S9), showing the great potential of the hydromechanical synthesis strategy in the controllable synthesis of many other 2D materials.

[1]Department of Materials Science and Engineering, City University of Hong Kong, Kowloon 999077, Hong Kong SAR, China

[2]State Key Laboratory of Infrared Physics, Shanghai Institute of Technical Physics, Chinese Academy of Sciences, Shanghai 200083, China

[3]Institute for Materials Chemistry and Engineering, Kyushu University, Fukuoka 816-8580, Japan

[4]State Key Laboratory of Terahertz and Millimeter Waves, City University of Hong Kong, Kowloon 999077, Hong Kong SAR, China

[5]Lead contact

*Correspondence: wdhu@mail.sitp.ac.cn (W.H.), johnnyho@cityu.edu.hk (J.C.H.)

https://doi.org/10.1016/j.matt.2024.04.013

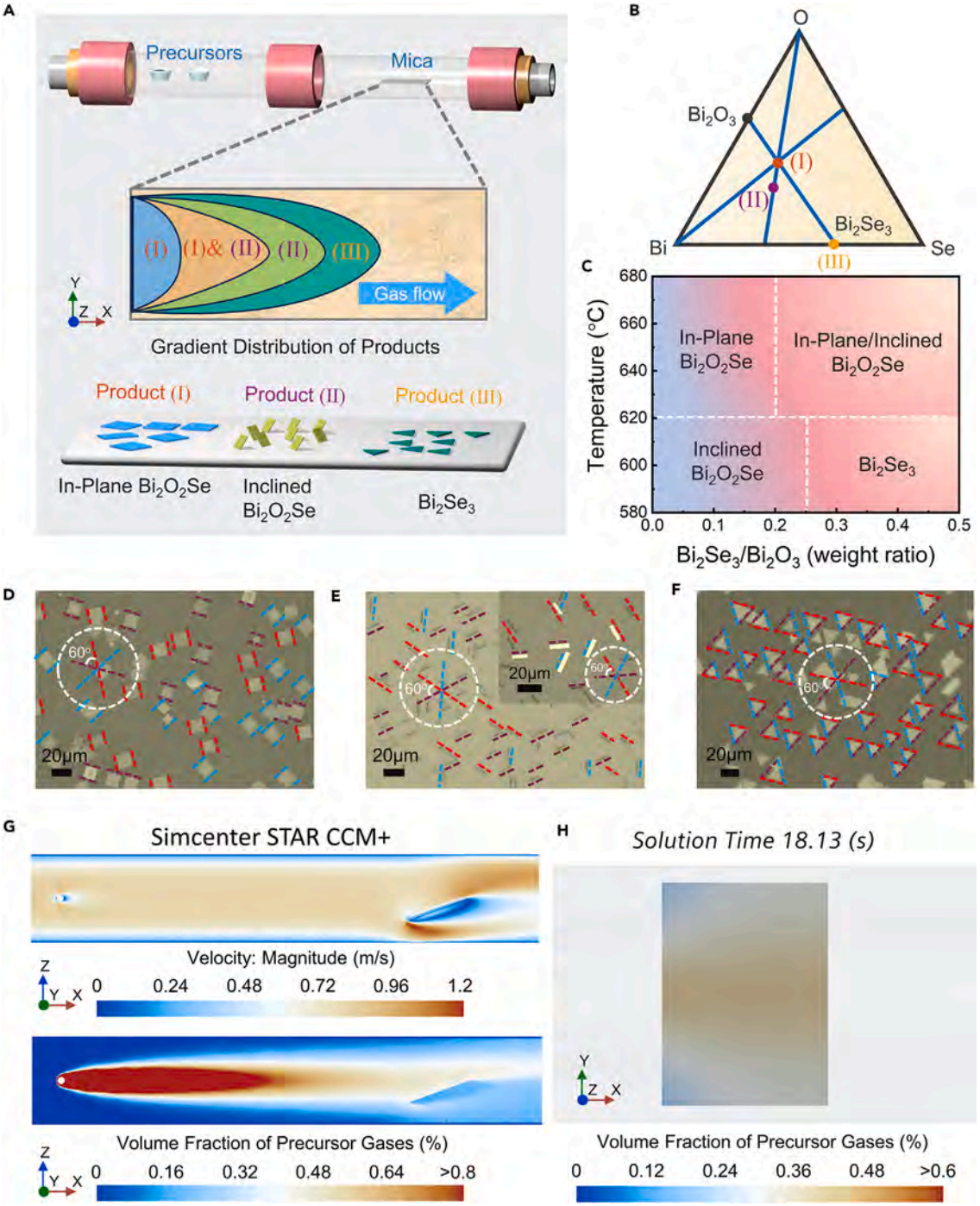

Figure 1. Hydromechanical strategy for aligned 2D material growth

(A) Schematic illustration of a conventional CVD system exhibiting the spatial sectioning of the growth substrate for (I) in-plane Bi_2O_2Se, (II) inclined Bi_2O_2Se, and (III) Bi_2Se_3, respectively.

(B) Schematic representation of the Bi–O–Se ternary phase diagram.

(C) Summary of the Bi–O–Se products via regulating the temperatures and weight ratios of Bi_2Se_3 and Bi_2O_3 precursors.

(D–F) Optical microscope images of the well-orientated single-crystalline 2D islands along the high-symmetry direction. The crystallographic orientations of 2D material flakes are positioned in red, blue, and purple colors, respectively. Compared to the conventional CVD synthesis system (Figure S1), the hydrodynamics system demonstrates excellent controllability by yielding a specific single product without misorientation, showcasing its superiority.

Figure 1. *Continued*
(G) Simulated distribution of the carrier gas velocity (top) and the precursor concentration field (bottom) using Simcenter STAR CCM+ software for a hydromechanical CVD system.
(H) Simulated precursor concentration (~4% on average) on the top surface of the substrate at equilibrium with a solution time of 18.13 s.

It is essential to mention that although enormous research efforts have been devoted to Bi_2O_2Se synthesis, this is the first report on the preferentially aligned growth of in-plane Bi_2O_2Se nanoflakes on a substrate. A series of Simcenter STAR CCM+ simulations are performed for the conventional and hydrodynamic systems, keeping all other growth parameters constant, such as growth temperature, pressure, etc., to semiquantitatively compare their controllability of precursor transport (Figures S10–S12). The simulations highlight the significance of flow rate and precursor concentration across the growth substrate in a CVD reactor, providing strong evidence for robustly achieving the aligned growth of 2D materials in the hydrodynamics system. Figures 1G and 1H show the simulated result of carrier gas velocity and precursor concentration with the titled angle of 20° and a solution time of 17.17 s, respectively. The result indicates that both gas flow velocity and precursor concentration near the mica substrate are effectively regulated since the titled mica substrate (length × width = 2 × 1.8 cm) can serve as a "valve" owing to the limited tube size (1 inch). More importantly, a lower precursor concentration dissipation is obtained for the hydrodynamic CVD system, compared to the conventional CVD system, with respect to the point source, demonstrating better controllability of the vapor precursor by simply regulating the valve angle. The above simulation results support our experimental observations and highlight the importance of deliberate process management to achieve a controllable synthesis of 2D materials in the CVD method by manipulating process parameters and reactor geometry.

Characteristics of the aligned 2D materials

The morphology and crystal structure of the 2D Bi–O–Se products are then investigated by a combination of experimental techniques. The atomic force microscopy (AFM) images of the 2D Bi–O–Se products are shown in Figures 2A–2C, revealing a clean and atomically flat surface topography with root-mean-square surface roughness of 5.08, 5.12, and 5.25 Å, respectively, within the area of 2 × 2 μm. Adopting the hydrodynamic strategy, the 2D Bi–O–Se products exhibit significantly improved controllability, with characteristic average thicknesses of ~7.2 nm for in-plane Bi_2O_2Se, ~20.9 nm for tilted Bi_2O_2Se, and ~7.1 nm for Bi_2Se_3 (Figures 2D–2F). Figure 2G exhibits that X-ray diffraction (XRD) measurements of in-plane Bi_2O_2Se,[29] inclined Bi_2O_2Se,[30] and Bi_2Se_3[31] are well aligned with the precious works. Notably, the tilted Bi_2O_2Se shows an additional (013) peak in the XRD measurements corresponding to the (013) crystal planes from the cross-sectional scanning transmission electron microscope images via focused ion beam sectioning.[30] The unmarked diffraction peaks originated from the pristine mica substrate match well with the standard XRD card PDF no. 16-0344 (Figure S13). X-ray photoelectron spectroscopy (XPS) reveals the chemical bonding states of Bi and Se for the in-plane/flat Bi_2O_2Se and Bi_2Se_3 (Figure S14), and all the resolved peaks are consistent with the composition of previous works.[32,33] The inclined Bi_2O_2Se flakes are converted into flat ones for XPS measurements through proper ultrasonication since the XPS instrument can only analyze ~5–10 nm of the top surface,[34] making the signal intensity of inclined samples too weak for identification. Figures 2H and 2I display the related Raman spectra and optical analysis of each 2D product, which are well-aligned with their characteristic vibration peaks.[30,35–37] Compared to in-plane or flat Bi_2O_2Se flakes, a relatively large redshift of the A_{1g} peak for the inclined Bi_2O_2Se is observed, which could be attributed to the inharmonicity of lattice vibrations.[38] (Note S2) The above

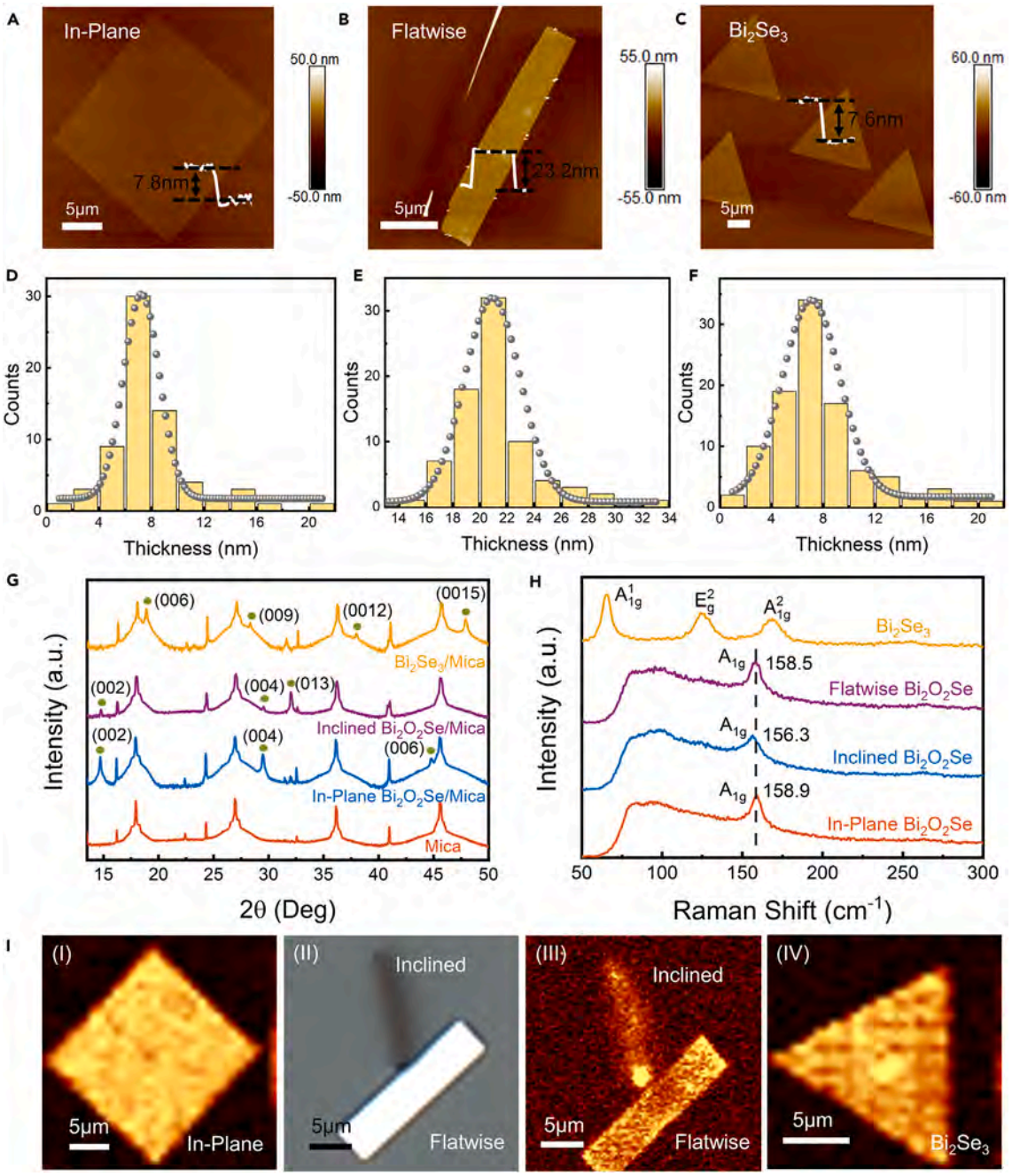

Figure 2. Characterization of the aligned 2D materials

(A–C) AFM measurements of 2D Bi–O–Se flakes with feature thicknesses of 7.8 (in-plane Bi_2O_2Se), 23.2 (inclined Bi_2O_2Se), and 7.6 nm (Bi_2Se_3), respectively.

(D–F) Average thickness distribution of the well-aligned Bi–O–Se flakes on mica substrate: in-plane Bi_2O_2Se (~7.2 nm), inclined Bi_2O_2Se (~20.9 nm), and Bi_2Se_3 flakes (~7.1 nm), respectively.

(G) XRD patterns of the pristine mica substrate and as-grown 2D Bi–O–Se flakes on mica substrates.

(H) Raman spectra of different 2D Bi–O–Se products on mica substrates. Meanwhile, flatwise Bi_2O_2Se flakes refer to the inclined Bi_2O_2Se flakes after 2 s of ultrasound.

(I) Optical measurements of the related 2D flakes. (I) Raman mapping of the as-grown Bi_2O_2Se A_{1g} peak. (II and III) Optical microscope image and corresponding Raman mapping of Bi_2O_2Se A_{1g} peak for the inclined and flat Bi_2O_2Se, respectively. (IV) Raman mapping of the as-grown Bi_2Se_3 A_{1g} peak.

analyses demonstrate that our 2D products synthesized by hydrodynamic strategy via the CVD method are of high quality with excellent uniformity, stoichiometry, crystallinity, etc.

Insight into the epitaxy relationship with vdWs dielectrics

Experimental observations indicate that the alignment of a 2D material on the mica substrate is synergistically influenced by the symmetries of the material itself and the underlying substrate. Thus, a comprehensive theory on 2D materials epitaxy, capable of predicting the alignment of various 2D products on mica substrates, is highly desirable as an experimental design guideline for large-scale 2D film synthesis. However, no general theory exists to explain the epitaxial relationship between different 2D materials on mica. Thanks to the weak bonding between the potassium (K) ions and aluminosilicate layers, vdWs mica dielectrics possess a perfect cleavage parallel to {001} planes,[39] which is intrinsically favorable for the lateral migration of precursor atoms and epitaxial growth of 2D materials.[40] The {001} cleavage planes, consisting of the K ions, with an ideal surface, possess a 6-fold rotational symmetry (C_6) (Figure S15), and the alignment of 2D materials with self-passivated edges on mica substrate is dominated by the weak vdWs forces.[41,42] In such scenery, the interaction between 2D materials and mica {001} planes is required to reveal the alignment of 2D materials on mica by utilizing the periodic boundary condition models. Previous studies have shown that 2D materials (edges of graphene, h-BN, and transition-metal dichalcogenides [TMDCs]) tend to align their high-symmetry directions with those of their substrates, such as the <110> directions of Cu (111),[43] <11–20> of h-BN[44], and (0001) planes of Al_2O_3.[45] This rule is consistent with our experimental observations on the epitaxial growth of in-plane Bi_2O_2Se, inclined Bi_2O_2Se, and Bi_2Se_3 on mica substrates (Figures 1D–1F), as well as being in perfect agreement with many experimental observations on 2D materials' growth on the vdWs mica dielectrics known up to now (Table S1).

To verify the assumption that a 2D material tends to align its high-symmetry direction with the high-symmetry direction of the mica surface, comprehensive DFT calculations are conducted based on our well-aligned 2D materials synthesis. Figures 3A–3C exhibit the schematic models of our 2D materials clusters aligning along the high-symmetry directions of the mica dielectric for the related DFT calculations. In the calculations, various angles between different 2D material clusters regarding vdWs mica dielectrics are modeled to ensure the accuracy of the calculations (Figures S16–S18). Detailed methods for calculations are provided in the experimental procedures. Figure 3D shows the binding energy of different 2D material clusters on a mica substrate as a function of the alignment angle between the self-passivated edges of 2D materials and the high-symmetry <110> direction of the mica {001} surface. These results show that the system's overall energy maintains the lowest value when the self-passivated edges of the 2D materials follow the high-symmetry direction of the neighboring vdWs substrate. Although we calculate very limited epitaxial systems of 2D materials on mica, the above results allow us to summarize the rule for the alignment of an arbitrary 2D material on mica, i.e., a high-symmetry direction of the 2D island prefers to align along a high-symmetry direction of the mica substrate.

With the principle that determines the alignment of an arbitrary 2D material on a mica substrate established, we will further discuss how the symmetries of both the substrate and the 2D material interact in the epitaxial growth. Considering a 2D material with a G_{2D} symmetry group placed on a 6-fold mica substrate (G_{Mica}), the symmetry group of the system, $G_{2D\&Mica}$, must be a subgroup of either G_{2D} or G_{Mica} because the alignment of the 2D material and the substrate remains unaffected by any symmetry operation of $G_{2D\&Mica}$. As derived in Note S3, the number of

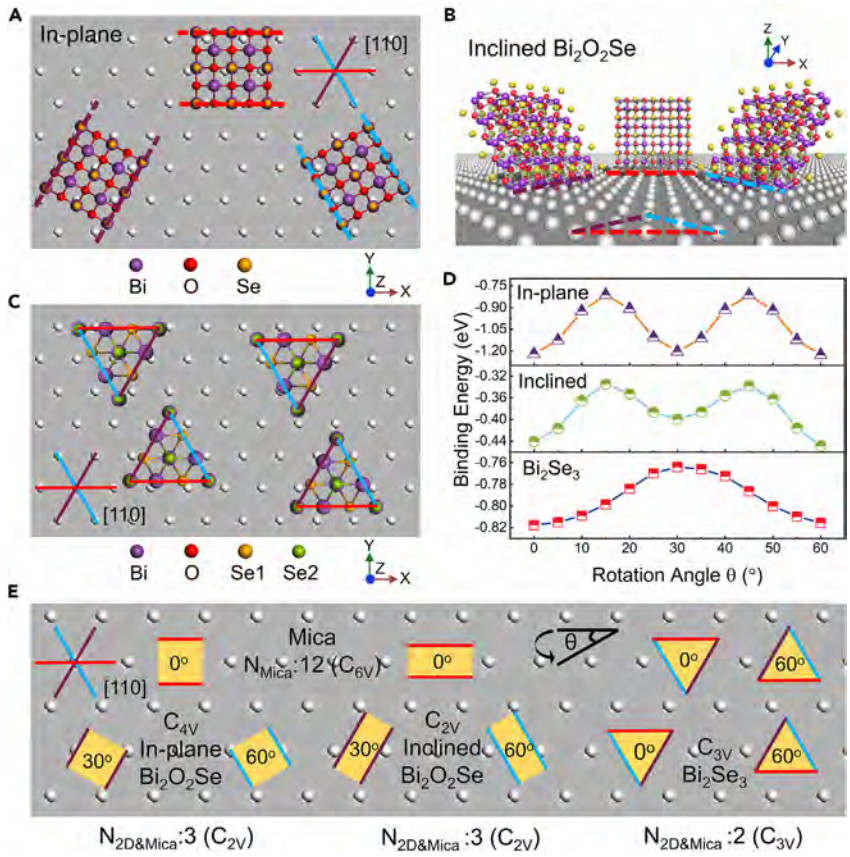

Figure 3. Study on the epitaxy relationship with vdWs dielectrics

(A–C) Schematic model of 2D materials clusters aligning along the high-symmetry direction of the mica dielectric.

(D) The calculated binding energies of the 2D materials cluster on the mica surface as a function of the alignment angle (θ) between a high-symmetry direction of 2D materials and a high-symmetry mica surface.

(E) The number of equivalent but distinct alignments of our experimental 2D products on the mica substrate. The symmetry groups of the mica substrate, 2D materials, and the system of the 2D island on mica are provided. The number of symmetry operations of the mica substrate and the whole system are N_{Mica} and $N_{2D\&Mica}$, respectively. Consistent with our experimental observations, these 2D products, including in-plane Bi_2O_2Se, inclined Bi_2O_2Se, and Bi_2Se_3, exhibit 3, 3, and 2 equivalent but different orientations, respectively.

equivalent but distinct directions of a 2D material on mica {001} surfaces, defined as N_E, can be computed using the following formula, derived from Lagrange's theorem of the group theory[46,47]:

$$N_E = \frac{|G_{Mica}|}{|G_{2D\&Mica}|},$$

where $|G_{Sub}|$ and $|G_{2D\&Mica}|$ are the numbers of distinct symmetry operations of G_{Sub} and $G_{2D\&Sub}$, respectively. According to the abovementioned principle of arbitrary 2D materials on mica, a high-symmetry edge of a 2D material preferably aligned along a high-symmetry direction of the mica substrate, the symmetry group of the whole system, $G_{2D\&Mica}$, must be the largest subgroup of both G_{Mica} and G_{2D}. Given all possible combinations of the symmetries of the 2D material and the mica substrate, the number of equivalent but distinct alignments of various 2D materials on mica {001} surfaces are summarized (Table 1). Consequently, according to our

Table 1. Summary of the number of equivalents

G_{2D}	C_{6V}	C_{4V}	C_{3V}	C_{2V}
G_{Mica}	C_{6V}	C_{6V}	C_{6V}	C_{6V}
$G_{2D\&Mica}$	C_{6V}	C_{2V}	C_{3V}	C_{2V}
$\|G_{Mica}\|$	12	12	12	12
$\|G_{2D\&Mica}\|$	12	4	6	4
N_E	1	3	2	3

The number of equivalent but different orientations of a 2D material on a mica substrate is based on the interplay between their symmetries.

experimental observation and theoretical analysis (Figure 3E), we believe that the N_E for most 2D materials synthesized on mica can be reasonably predicted, providing a desirable experimental design guideline before the general synthesis of 2D materials on the vdWs mica dielectric.

High-precision manipulation of the vdWs dielectric

After demonstrating the superiority of the oriented growth of 2D materials, device-level implementations based on as-grown 2D materials/vdWs dielectrics to reveal the "true" properties of as-grown 2D materials are further explored, utilizing vdWs mica/SiO_2 as the hybrid dielectric layers. Figure 4A illustrates the device fabrication process of the FETs, in which a high-fidelity transfer method is developed by utilizing the thermal releasing tape to assist in the fabrication of hybrid mica/SiO_2 dielectric layers. Figure 4B depicts the schematic of the backgated FET, and its optical and AFM images demonstrate the thicknesses of the Bi_2O_2Se layer and mica dielectric layer with atomic-scale flatness as 3.4 and ~100 nm, respectively (Figure S19). It is worth mentioning that the thickness of the as-grown Bi_2O_2Se/vdWs mica dielectric heterostructures is controlled by the exfoliation time with blue tape before thermally releasing onto SiO_2. As shown in Figure 4C, the corresponding transfer curves of the device on a logarithmic scale reveal a record-high current on/off ratio of 1.4×10^7 at a relatively small source/drain bias of V_{DS} = 20 mV. Figure 4D exhibits the linear output curves of the device at V_{GS} sweeping from −15 to 15 V, demonstrating the ohmic contact between the Bi_2O_2Se semiconductor channel and Au electrodes.

Compared to many state-of-the-art 2D-material-channeled FETs integrated with various dielectrics (Figure 4E), our Bi_2O_2Se-based FETs with hybrid mica/SiO_2 gate dielectrics show high mobility of 22.3 ± 1.2 $cm^2 V^{-1} S^{-1}$ for a channel thickness down to 3.4 nm of about 6 layers (Figures S20 and S21), which is superior or comparable to the most widely investigated non-vdWs dielectrics, e.g., Al_2O_3, SiO_2, HfO_2, etc. (Table S2). This high carrier mobility of the ultrathin Bi_2O_2Se flake not only demonstrates the high quality of our CVD-grown ultrathin 2D Bi_2O_2Se materials but also shows the low interface trap density and coulomb impurity concentration as compared to the other device techniques (Figures S22–S24). Figure 4F gives the high current on/off ratio (1.4×10^7) of our Bi_2O_2Se FETs, which is significantly better or comparable to many promisingly 2D materials, including TMDCs, black phosphorus (BP), β-Ga_2O_3, etc., demonstrating the excellent coupling of as-grown Bi_2O_2Se flakes on the transferable hybrid dielectrics. By leveraging the as-grown Bi_2O_2Se on its original vdWs epitaxial dielectric, the FETs exhibit improved performance attributes and mitigate the detrimental effects that can arise from additional device fabrication steps, showing their superiority in reducing the performance degradation of the CVD-grown 2D semiconductors (Figure S25). Considering the high transparency, excellent flexibility, and suitable insulating properties of mica, this research lays the foundation for potential device-level studies on the transferable dielectric of mica, e.g., flexible transparent electronics.

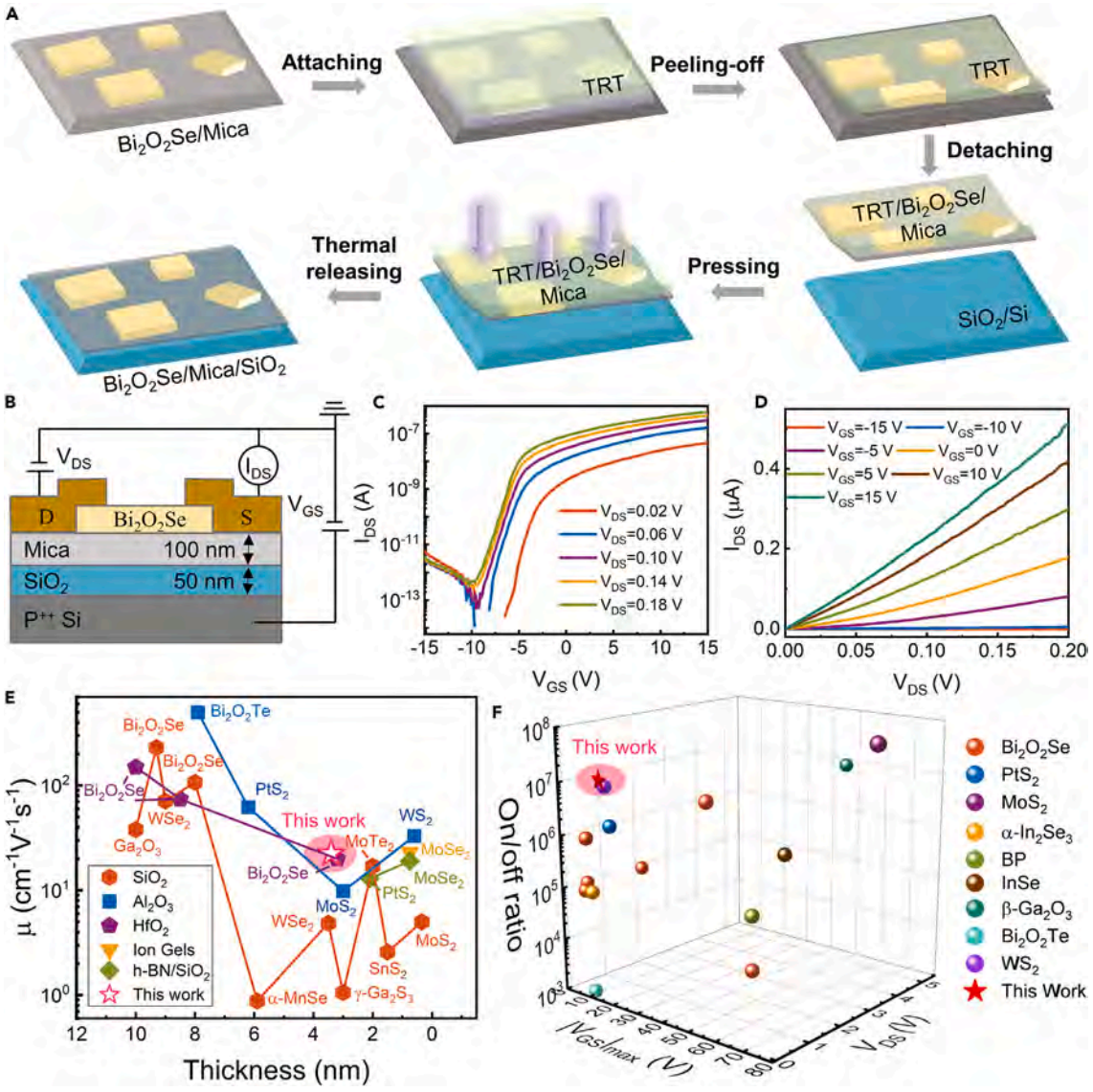

Figure 4. Device fabrication and performance evaluations

(A) Device fabrication process of the Bi_2O_2Se FETs using mica/SiO_2 as hybrid dielectric layers via a high-fidelity transfer method assisted by the thermal releasing tape (TRT).

(B) Schematic illustration of the back-gated FETs where the Bi_2O_2Se semiconductor and mica/SiO_2 hybrid layer are used as the transistor channel and gate dielectric, respectively.

(C) Transfer curves of the mica-based Bi_2O_2Se FETs as V_{DS} increases from 0.02–0.18 V, revealing typical n-type characteristics with a current on/off ratio of 1.4×10^7.

(D) Output characteristics of the Bi_2O_2Se FET as V_{GS} increases from −15 to 15 V.

(E) Mobility of our Bi_2O_2Se-based FETs with the hybrid mica/SiO_2 gate dielectric compared to other state-of-the-art 2D FETs integrated with various dielectrics.[48–65]

(F) On/off ratio of the device at a relatively small bias of V_{DS} = 0.02 V as gate voltages sweep from −15 to 15 V, and the performance comparison with the state-of-the-art 2D FETs based on distinct categories of 2D materials, e.g., TMDCs, BP, β-Ga_2O_3, etc.[30,48,57,60–70]

Conclusions

In summary, we investigate the aligned epitaxy of 2D materials and develop a method for the high-fidelity manipulation of as-grown 2D materials on the vdWs mica dielectric at the device level. The aligned epitaxy of distinct CVD-grown 2D materials is realized by adopting the hydromechanical strategy. Simcenter STAR

CCM+ simulation is employed to understand the enhanced precursor controllability during the CVD synthesis. In addition, the insight into the epitaxy relationship between our 2D products and vdWs mica dielectrics is uncovered by DFT calculations, demonstrating the energy-favorable directions of 2D clusters on mica dielectrics. Specifically, combined with Lagrange's theorem of the group theory, the number of equivalent but different directions of a 2D material on mica is first established, potentially applicable to many other 2D epitaxy systems. More importantly, detailed electrical device characterization is performed for the high-fidelity manipulation of the as-grown Bi_2O_2Se-based device with hybrid dielectrics, exhibiting a record high current on/off ratio of 1.4×10^7 and excellent carrier mobility of 22.4 $cm^2 V^{-1} S^{-1}$. Overall, this work provides a powerful methodology platform for synthesizing the aligned 2D materials, predicting the alignment direction, evaluating their intrinsic properties, and laying the foundation for probing device functionalities, e.g., flexible transparent electronics.

EXPERIMENTAL PROCEDURES

Resource availability

Lead contact

Further information and requests for resources and reagents should be directed to and will be fulfilled by the lead contact, Johnny C. Ho (johnnyho@cityu.edu.hk).

Materials availability

This study did not generate new unique reagents.

Data and code availability

Any additional information required to reanalyze the data reported in this paper is available from the lead contact upon request.

MATERIALS SYNTHESIS AND CHARACTERIZATION

Bi_2O_2Se flakes were synthesized by the CVD method using Bi_2Se_3 (Aldrich, 99.99%) and Bi_2O_3 (Thermo Scientific, 98%) powders as the precursors.[71,72] The quartz boat of the Bi_2O_3 side was put in the center of the heating zone, and the mica substrate was placed at a proper downstream position accordingly. The furnace was heated to 635°C–650°C with a ramping time of 10 min and a holding time of 10–25 min under ~124 torr. Ahead of the heating process, the furnace tube was flushed with high-purity argon gas to thoroughly exhaust the atmospheric moisture and oxygen. After high-temperature deposition, the furnace was naturally cooled to room temperature. The topological morphologies of the materials were characterized by optical and atomic force microscopes (Dimension Icon, Bruker). Raman spectra were collected by a confocal microscope spectrometer (Alpha 300R, WITec).

Simcenter STAR CCM+ simulation

As the flow velocity in the tubular furnace remains relatively flat, a laminar flow model coupled with dilute material transfer modules was selected to simplify the numerical computation for mass transport in the CVD systems. The detailed models for the related Simcenter STAR CCM+ simulation are shown in Figure S26. Except for the basic geometries of the two systems, other key parameters, e.g., pressure, carrier gas, etc., were consistent with the experimental condition provided in the materials synthesis and characterization section. It is worth noting that the precursor with a volume fraction of precursor gases (1%) was viewed as a continuous point source diffusion model (which is denoted as a normalized unit concentration). A balanced concentration distribution of the precursor vapor on growth substrates was obtained using the computational fluid dynamics solver.

DFT calculations of the binding energies

The DFT calculations were performed with the Vienna Ab-initio Simulation Package code with the full-potential projected augmented wave formalism.[73,74] The generalized gradient approximation of the Perdew-Burke-Ernzerhof functional was used to describe the exchange and correlation functions.[75] The structure was relaxed until the atomic force was less than 0.01 eV $Å^{-1}$, and the self-consistent calculation was terminated when the energy converged to 10^{-4} eV. A 2 × 2 unit cell of mica and a 2 × 2 unit cell of Bi_2O_2Se or Bi_2Se_3 were constructed to match each other. To eliminate the perturbation from neighboring slabs, a vacuum layer of 20 Å was used. The vdWs interaction between matched layers was considered by the DFT-D3 method of Grimme with a zero-damping function.[76] The cutoff energy for the plane-wave expansion was set to 450 eV, and a k-point mesh of 3 × 3 × 1 was employed to sample the Brillouin zone.

To separately calculate the interaction between 2D products (in-plane Bi_2O_2Se, inclined Bi_2O_2Se, and Bi_2Se_3 nanoflakes), different pristine clusters with their typical geometry shapes were stacked onto a mica (001) surface under periodic boundary conditions and with different alignment angles (5° per step). During the geometry optimization, the top atomic layer of the K metal slab was fixed, as the edges of the clusters are generally self-passivated. The binding energy between the calculated 2D materials and the mica substrate is defined as

$$E_b = E_{total} - E_{2D} - E_{mica},$$

where E_{total}, E_{2D}, and E_{mica} are the energies of the whole system, the 2D materials layer, and the mica substrate, respectively.

Device fabrication and evaluation

For the back-gated FETs, the as-grown Bi_2O_2Se flakes were detached from mica and transferred to the desired dielectric substrate by a poly(methyl methacrylate) (PMMA)-assisted wet-transfer method (Figure S13). The Au electrodes were patterned by electron-beam lithography and thermally evaporated with a thickness of 40 nm. The electronic performance was characterized by a semiconductor analyzer (Agilent 4155C) and probe station.

SUPPLEMENTAL INFORMATION

Supplemental information can be found online at https://doi.org/10.1016/j.matt.2024.04.013.

ACKNOWLEDGMENTS

This research was financially supported by a fellowship award from the Research Grants Council of the Hong Kong Special Administrative Region, China (CityU RFS2021-1S04), and the Shenzhen Municipality Science and Technology Innovation Commission (grant no. SGDX2020110309300402 ["Modulation and Detection of Terahertz Waves based on Semi-Metallic Two-Dimensional Materials," CityU]).

AUTHOR CONTRIBUTIONS

Weijun Wang, Y.Z., and Wei Wang contributed equally to this work. J.C.H. and Weijun Wang conceived the project. Y.Z. and Wei Wang performed the DFT calculations and Simcenter STAR CCM+ simulation. Weijun Wang, Y.Z., and Wei Wang conducted AFM, Raman, and XPS characterization and analysis. Weijun Wang, M.L., and Y.M. fabricated the devices and performed the electrical tests and data processing. B.L., Y.Y., D.Y., P.X., D.L., D.C., Q.Q., and S.Y. helped to prepare the samples and

perform the basic material characterizations. W.H., J.C.H., and Weijun Wang wrote the paper. All authors reviewed and commented on the manuscript.

DECLARATION OF INTERESTS

The authors declare no competing interests.

Received: January 3, 2024
Revised: February 23, 2024
Accepted: April 7, 2024
Published: May 7, 2024

REFERENCES

1. Aljarb, A., Fu, J.H., Hsu, C.C., Chuu, C.P., Wan, Y., Hakami, M., Naphade, D.R., Yengel, E., Lee, C.J., Brems, S., et al. (2020). Ledge-directed epitaxy of continuously self-aligned single-crystalline nanoribbons of transition metal dichalcogenides. Nat. Mater. *19*, 1300. https://doi.org/10.1038/s41563-020-0795-4.

2. Nguyen, V.L., Shin, B.G., Duong, D.L., Kim, S.T., Perello, D., Lim, Y.J., Yuan, Q.H., Ding, F., Jeong, H.Y., Shin, H.S., et al. (2015). Seamless Stitching of Graphene Domains on Polished Copper (111) Foil. Adv. Mater. *27*, 1376–1382. https://doi.org/10.1002/adma.201404541.

3. Dean, C.R., Young, A.F., Meric, I., Lee, C., Wang, L., Sorgenfrei, S., Watanabe, K., Taniguchi, T., Kim, P., Shepard, K.L., and Hone, J. (2010). Boron nitride substrates for high-quality graphene electronics. Nat. Nanotechnol. *5*, 722–726. https://doi.org/10.1038/nnano.2010.172.

4. Khan, U., Luo, Y., Tang, L., Teng, C., Liu, J., Liu, B., and Cheng, H.M. (2019). Controlled Vapor Solid Deposition of Millimeter-Size Single Crystal 2D Bi_2O_2Se for High-Performance Phototransistors. Adv. Funct. Mater. *29*, 1807979. https://doi.org/10.1002/adfm.201807979.

5. Tong, T., Chen, Y., Qin, S., Li, W., Zhang, J., Zhu, C., Zhang, C., Yuan, X., Chen, X., Nie, Z., et al. (2019). Sensitive and Ultrabroadband Phototransistor Based on Two-Dimensional Bi_2O_2Se Nanosheets. Adv. Funct. Mater. *29*, 1905806. https://doi.org/10.1002/adfm.201905806.

6. Rhodes, D., Chae, S.H., Ribeiro-Palau, R., and Hone, J. (2019). Disorder in van der Waals heterostructures of 2D materials. Nat. Mater. *18*, 541–549. https://doi.org/10.1038/s41563-019-0366-8.

7. Chen, J.H., Jang, C., Xiao, S., Ishigami, M., and Fuhrer, M.S. (2008). Intrinsic and extrinsic performance limits of graphene devices on SiO. Nat. Nanotechnol. *3*, 206–209. https://doi.org/10.1038/nnano.2008.58.

8. Raja, A., Waldecker, L., Zipfel, J., Cho, Y., Brem, S., Ziegler, J.D., Kulig, M., Taniguchi, T., Watanabe, K., Malic, E., et al. (2019). Dielectric disorder in two-dimensional materials. Nat. Nanotechnol. *14*, 832–837. https://doi.org/10.1038/s41565-019-0520-0.

9. Chen, T.A., Chuu, C.P., Tseng, C.C., Wen, C.K., Wong, H.S.P., Pan, S., Li, R., Chao, T.A., Chueh, W.C., Zhang, Y., et al. (2020). Wafer-scale single-crystal hexagonal boron nitride monolayers on Cu (111). Nature *579*, 219–223. https://doi.org/10.1038/s41586-020-2009-2.

10. Xu, Y., Liu, T., Liu, K., Zhao, Y., Liu, L., Li, P., Nie, A., Liu, L., Yu, J., Feng, X., et al. (2023). Scalable integration of hybrid high- dielectric materials on two-dimensional semiconductors. Nat. Mater. *22*, 1078–1084. https://doi.org/10.1038/s41563-023-01626-w.

11. Chen, J., Liu, Z., Dong, X., Gao, Z., Lin, Y., He, Y., Duan, Y., Cheng, T., Zhou, Z., Fu, H., et al. (2023). Vertically grown ultrathin Bi_2SiO_5 as high-κ single-crystalline gate dielectric. Nat. Commun. *14*, 4406. https://doi.org/10.1038/s41467-023-40123-1.

12. An, L., Yu, Y., Cai, Q., Mateti, S., Li, L.H., and Chen, Y.I. (2023). Hexagonal boron nitride nanosheets: Preparation, heat transport property and application as thermally conductive fillers. Prog. Mater. Sci. *138*, 101154. https://doi.org/10.1016/j.pmatsci.2023.101154.

13. Liu, K., Jin, B., Han, W., Chen, X., Gong, P., Huang, L., Zhao, Y., Li, L., Yang, S., Hu, X., et al. (2021). A wafer-scale van der Waals dielectric made from an inorganic molecular crystal film. Nat. Electron. *4*, 906–913. https://doi.org/10.1038/s41928-021-00683-w.

14. Takenobu, T. (2023). High-κ two-dimensional dielectric. Nat. Mater. *22*, 811–812. https://doi.org/10.1038/s41563-023-01567-4.

15. Ji, Q., Zhang, Y., Gao, T., Zhang, Y., Ma, D., Liu, M., Chen, Y., Qiao, X., Tan, P.-H., Kan, M., et al. (2013). Epitaxial monolayer MoS_2 on mica with novel photoluminescence. Nano Lett. *13*, 3870–3877. https://doi.org/10.1021/nl401938t.

16. Wu, Z., Tai, G., Liu, R., Hou, C., Shao, W., Liang, X., and Wu, Z. (2021). van der Waals Epitaxial Growth of Borophene on a Mica Substrate toward a High-Performance Photodetector. ACS Appl. Mater. Inter. *13*, 31808–31815. https://doi.org/10.1021/acsami.1c03146.

17. Qin, J.-K., Shao, W.-Z., Li, Y., Xu, C.-Y., Ren, D.-D., Song, X.-G., and Zhen, L. (2017). van der Waals epitaxy of large-area continuous ReS_2 films on mica substrate. RSC Adv. *7*, 24188–24194. https://doi.org/10.1039/C7RA01748K.

18. Qin, B., Ma, H., Hossain, M., Zhong, M., Xia, Q., Li, B., and Duan, X. (2020). Substrates in the synthesis of two-dimensional materials via chemical vapor deposition. Chem. Mater. *32*, 10321–10347. https://doi.org/10.1021/acs.chemmater.0c03549.

19. Wang, N., Pan, X., Wang, P., Wang, Y., He, H., Zeng, Y.-J., Zhang, L., Li, Y., Wang, F., Lu, B., et al. (2022). Is all epitaxy on mica van der Waals epitaxy? Mater. Today Nano *20*, 100255. https://doi.org/10.1016/j.mtnano.2022.100255.

20. Zhang, X., He, Y., Li, R., Dong, H., and Hu, W. (2016). 2D Mica Crystal as Electret in Organic Field-Effect Transistors for Multistate Memory. Adv. Mater. *28*, 3755–3760. https://doi.org/10.1002/adma.201506356.

21. Weeks, J.R. (1922). The dielectric constant of mica. Phys. Rev. *19*, 319–322. https://doi.org/10.1103/PhysRev.19.319.

22. Frisenda, R., Niu, Y., Gant, P., Muñoz, M., and Castellanos-Gomez, A. (2020). Naturally occurring van der Waals materials. Npj 2d Mater. Appl. *4*, 38. https://doi.org/10.1038/s41699-020-00172-2.

23. Low, C.G., Zhang, Q., Hao, Y., and Ruoff, R.S. (2014). Graphene Field Effect Transistors with Mica as Gate Dielectric Layers. Small *10*, 4213–4218. https://doi.org/10.1002/smll.201303929.

24. Wang, S., Li, Y., Ng, A., Hu, Q., Zhou, Q., Li, X., and Liu, H. (2020). 2D Bi2Se3 van der Waals epitaxy on mica for optoelectronics applications. Nanomater *10*, 1653. https://doi.org/10.3390/nano10091653.

25. Khan, U., Luo, Y., Tang, L., Teng, C., Liu, J., Liu, B., and Cheng, H.M. (2019). Controlled vapor–solid deposition of millimeter-size single crystal 2D Bi_2O_2Se for high-performance phototransistors. Adv. Funct. Mater. *29*, 1807979. https://doi.org/10.1002/adfm.201807979.

26. Ling, X., Lee, Y.H., Lin, Y., Fang, W., Yu, L., Dresselhaus, M.S., and Kong, J. (2014). Role of the Seeding Promoter in MoS2 Growth by Chemical Vapor Deposition. Nano Lett. *14*, 464–472. https://doi.org/10.1021/nl4033704.

27. van der Zande, A.M., Huang, P.Y., Chenet, D.A., Berkelbach, T.C., You, Y., Lee, G.H., Heinz, T.F., Reichman, D.R., Muller, D.A., and Hone, J.C. (2013). Grains and grain boundaries in highly crystalline monolayer molybdenum disulphide. Nat. Mater. *12*, 554–561. https://doi.org/10.1038/nmat3633.

28. Govind Rajan, A., Warner, J.H., Blankschtein, D., and Strano, M.S. (2016). Generalized Mechanistic Model for the Chemical Vapor Deposition of 2D Transition Metal Dichalcogenide Monolayers. ACS Nano *10*,

4330–4344. https://doi.org/10.1021/acsnano.5b07916.

29. Wu, J., Tan, C., Tan, Z., Liu, Y., Yin, J., Dang, W., Wang, M., and Peng, H. (2017). Controlled Synthesis of High-Mobility Atomically Thin Bismuth Oxyselenide Crystals. Nano Lett. *17*, 3021–3026. https://doi.org/10.1021/acs.nanolett.7b00335.

30. Hong, C., Tao, Y., Nie, A., Zhang, M., Wang, N., Li, R., Huang, J., Huang, Y., Ren, X., Cheng, Y., and Liu, X. (2020). Inclined Ultrathin Bi2O2Se Films: A Building Block for Functional van der Waals Heterostructures. ACS Nano *14*, 16803–16812. https://doi.org/10.1021/acsnano.0c05300.

31. Wang, W., Geng, Y., Qian, Y., Xie, Y., and Liu, X. (1999). Synthesis and characterization of nanocrystalline Bi_2Se_3 by solvothermal method. Mater. Res. Bull. *34*, 131–134. https://doi.org/10.1016/S0025-5408(98)00203-7.

32. Messalea, K.A., Zavabeti, A., Mohiuddin, M., Syed, N., Jannat, A., Atkin, P., Ahmed, T., Walia, S., McConville, C.F., Kalantar-Zadeh, K., et al. (2020). Two-Step Synthesis of Large-Area 2D Bi_2S_3 Nanosheets Featuring High In-Plane Anisotropy. Adv. Mater. Interfaces *7*, 2001131. https://doi.org/10.1002/admi.202001131.

33. Khan, U., Nairan, A., Khan, K., Li, S., Liu, B., and Gao, J. (2023). Salt-Assisted Low-Temperature Growth of 2D Bi_2O_2Se with Controlled Thickness for Electronics. Small *19*, 2206648. https://doi.org/10.1002/smll.202206648.

34. Hossain, M.T., Jena, T., Nath, U., Sarma, M., and Giri, P.K. (2023). Room temperature exciton formation and robust optical properties of CVD-grown ultrathin Bi_2O_2Se crystals on arbitrary substrates. Nanoscale *15*, 11222–11236. https://doi.org/10.1039/d3nr01201h.

35. Yu, J., Han, Y., Zhang, H., Ding, X., Qiao, L., and Hu, J. (2022). Excimer Formation in the Non-Van-Der-Waals 2D Semiconductor Bi_2O_2Se. Adv. Mater. *34*, 2204227. https://doi.org/10.1002/adma.202204227.

36. Chen, Y., Ma, W., Tan, C., Luo, M., Zhou, W., Yao, N., Wang, H., Zhang, L., Xu, T., Tong, T., et al. (2021). Broadband Bi_2O_2Se Photodetectors from Infrared to Terahertz. Adv. Funct. Mater. *31*, 2009554. https://doi.org/10.1002/adfm.202009554.

37. Zhang, J., Peng, Z., Soni, A., Zhao, Y., Xiong, Y., Peng, B., Wang, J., Dresselhaus, M.S., and Xiong, Q. (2011). Raman Spectroscopy of Few-Quintuple Layer Topological Insulator Bi2Se3 Nanoplatelets. Nano Lett. *11*, 2407–2414. https://doi.org/10.1021/nl200773n.

38. Han, M., Wu, S., Zhao, X., He, Q., Zhang, B., Xiong, W., Luo, X., and Zheng, Y. (2023). Raman Spectroscopy of the Trapezoidal Bi_2O_2Se. Adv. Opt. Mater. *11*, 2300344. https://doi.org/10.1002/adom.202300344.

39. Poppa, H., and Elliot, A. (1971). The surface composition of mica substrates. Surf. Sci. *24*, 149–163. https://doi.org/10.1016/0039-6028(71)90225-1.

40. Huang, L., Yu, Y., Li, C., and Cao, L. (2013). Substrate Mediation in Vapor Deposition Growth of Layered Chalcogenide Nanoplates: A Case Study of SnSe2. J. Phys. Chem. C *117*, 6469–6475. https://doi.org/10.1021/jp400274a.

41. Sang, X., Li, X., Zhao, W., Dong, J., Rouleau, C.M., Geohegan, D.B., Ding, F., Xiao, K., and Unocic, R.R. (2018). In situ edge engineering in two-dimensional transition metal dichalcogenides. Nat. Commun. *9*, 2051. https://doi.org/10.1038/s41467-018-04435-x.

42. Ren, X., Dong, J., Yang, P., Li, J., Lu, G., Wu, T., Wang, H., Guo, W., Zhang, Z., Ding, F., and Jin, C. (2019). Grain boundaries in chemical-vapor-deposited atomically thin hexagonal boron nitride. Phys. Rev. Mater. *3*, 014004. https://doi.org/10.1103/PhysRevMaterials.3.014004.

43. Dong, J., Zhang, L., Zhang, K., and Ding, F. (2018). How graphene crosses a grain boundary on the catalyst surface during chemical vapour deposition growth. Nanoscale *10*, 6878–6883. https://doi.org/10.1039/c7nr06840a.

44. Zhang, Z., Yang, X., Liu, K., and Wang, R. (2022). Epitaxy of 2D Materials toward Single Crystals. Adv. Sci. *9*, 2105201. https://doi.org/10.1002/advs.202105201.

45. Ji, Q., Kan, M., Zhang, Y., Guo, Y., Ma, D., Shi, J., Sun, Q., Chen, Q., Zhang, Y., and Liu, Z. (2015). Unravelling Orientation Distribution and Merging Behavior of Mono layer MoS2 Domains on Sapphire. Nano Lett. *15*, 198–205. https://doi.org/10.1021/nl503373x.

46. Humphreys, J.F. (1996). A Course in Group Theory (USA: Oxford University Press).

47. Dong, J., Zhang, L., Dai, X., and Ding, F. (2020). The epitaxy of 2D materials growth. Nat. Commun. *11*, 5862. https://doi.org/10.1038/s41467-020-19752-3.

48. Kim, T.S., Noh, G., Kwon, S., Kim, J.Y., Dhakal, K.P., Oh, S., Chai, H.J., Park, E., Kim, I.S., Lee, E., et al. (2024). Diffusion Control on the Van der Waals Surface of Monolayers for Uniform Bi-Layer MoS_2 Growth. Adv. Funct. Mater. 2312365. https://doi.org/10.1002/adfm.202312365.

49. Sebastian, A., Pendurthi, R., Choudhury, T.H., Redwing, J.M., and Das, S. (2021). Benchmarking monolayer MoS_2 and WS_2 field-effect transistors. Nat. Commun. *12*, 693. https://doi.org/10.1038/s41467-020-20732-w.

50. Chang, Y.H., Zhang, W., Zhu, Y., Han, Y., Pu, J., Chang, J.K., Hsu, W.T., Huang, J.K., Hsu, C.L., Chiu, M.H., et al. (2014). Monolayer MoSe2 Grown by Chemical Vapor Deposition for Fast Photodetection. ACS Nano *8*, 8582–8590. https://doi.org/10.1021/nn503287m.

51. Uchiyama, Y., Kutana, A., Watanabe, K., Taniguchi, T., Kojima, K., Endo, T., Miyata, Y., Shinohara, H., and Kitaura, R. (2019). Momentum-forbidden dark excitons in hBN-encapsulated monolayer MoS2. Npj 2d Mater. Appl. *3*, 26. https://doi.org/10.1038/s41699-019-0108-4.

52. Xu, L., Zhang, P., Jiang, H., Wang, X., Chen, F., Hu, Z., Gong, Y., Shang, L., Zhang, J., Jiang, K., and Chu, J. (2019). Large-Scale Growth and Field-Effect Transistors Electrical Engineering of Atomic-Layer SnS_2. Small *15*, 1904116. https://doi.org/10.1002/smll.201904116.

53. Shafi, A.M., Uddin, M.G., Cui, X., Ali, F., Ahmed, F., Radwan, M., Das, S., Mehmood, N., Sun, Z., and Lipsanen, H. (2023). Strain Engineering for Enhancing Carrier Mobility in $MoTe_2$ Field-Effect Transistors. Adv. Sci. *10*, 2303437. https://doi.org/10.1002/advs.202303437.

54. Li, L., Wang, W., Chai, Y., Li, H., Tian, M., and Zhai, T. (2017). Few-Layered PtS2 Phototransistor on h-BN with High Gain. Adv. Funct. Mater. *27*, 1701011. https://doi.org/10.1002/adfm.201701011.

55. Liu, H., Chen, L., Zhu, H., Sun, Q.Q., Ding, S.J., Zhou, P., and Zhang, D.W. (2020). Atomic layer deposited 2D MoS_2 atomic crystals: from material to circuit. Nano Res. *13*, 1644–1650. https://doi.org/10.1007/s12274-020-2787-8.

56. Zhou, N., Gan, L., Yang, R., Wang, F., Li, L., Chen, Y., Li, D., and Zhai, T. (2019). Nonlayered two-dimensional defective semiconductor γ-Ga_2S_3 toward broadband photodetection. ACS Nano *13*, 6297–6307. https://doi.org/10.1021/acsnano.9b00276.

57. Wu, J., Yuan, H., Meng, M., Chen, C., Sun, Y., Chen, Z., Dang, W., Tan, C., Liu, Y., Yin, J., et al. (2017). High electron mobility and quantum oscillations in non-encapsulated ultrathin semiconducting Bi_2O_2Se. Nat. Nanotechnol. *12*, 530–534. https://doi.org/10.1038/Nnano.2017.43.

58. Pudasaini, P.R., Oyedele, A., Zhang, C., Stanford, M.G., Cross, N., Wong, A.T., Hoffman, A.N., Xiao, K., Duscher, G., Mandrus, D.G., et al. (2018). High-performance multilayer WSe_2 field-effect transistors with carrier type control. Nano Res. *11*, 722–730. https://doi.org/10.1007/s12274-017-1681-5.

59. Zhou, N., Zhang, Z., Wang, F., Li, J., Xu, X., Li, H., Ding, S., Liu, J., Li, X., Xie, Y., et al. (2022). Spin Ordering Induced Broadband Photodetection Based on Two-Dimensional Magnetic Semiconductor α-MnSe. Adv. Sci. *9*, 2202177. https://doi.org/10.1002/advs.202202177.

60. Wang, Z., Wang, P., Wang, F., Ye, J., He, T., Wu, F., Peng, M., Wu, P., Chen, Y., Zhong, F., et al. (2020). A Noble Metal Dichalcogenide for High-Performance Field-Effect Transistors and Broadband Photodetectors. Adv. Funct. Mater. *30*, 1907945. https://doi.org/10.1002/adfm.201907945.

61. Ai, W., Chen, J., Dong, X., Gao, Z., He, Y., Liu, Z., Fu, H., Luo, F., and Wu, J. (2022). High Mobility and Quantum Oscillations in Semiconducting Bi_2O_2Te Nanosheets Grown by Chemical Vapor Deposition. Nano Lett. *22*, 7659–7666. https://doi.org/10.1021/acs.nanolett.2c02891.

62. Fu, Q., Zhu, C., Zhao, X., Wang, X., Chaturvedi, A., Zhu, C., Wang, X., Zeng, Q., Zhou, J., Liu, F., et al. (2019). Ultrasensitive 2D Bi_2O_2Se phototransistors on silicon substrates. Adv. Mater. *31*, 1804945. https://doi.org/10.1002/adma.201804945.

63. Tan, C., Tang, M., Wu, J., Liu, Y., Li, T., Liang, Y., Deng, B., Tan, Z., Tu, T., Zhang, Y., et al. (2019). Wafer-Scale Growth of Single-Crystal 2D Semiconductor on Perovskite Oxides for High-Performance Transistors. Nano Lett. *19*, 2148–2153. https://doi.org/10.1021/acs.nanolett.9b00381.

64. Wu, Z., Jiang, Z., Song, P., Tian, P., Hu, L., Liu, R., Fang, Z., Kang, J., and Zhang, T.Y. (2019).

Nanowire-Seeded Growth of Single-Crystalline (010) β-Ga_2O_3 Nanosheets with High Field-Effect Electron Mobility and On/Off Current Ratio. Small *15*, 1900580. https://doi.org/10.1002/smll.201900580.

65. Wang, L., Wang, X., Zhang, Y., Li, R., Ma, T., Leng, K., Chen, Z., Abdelwahab, I., and Loh, K.P. (2020). Exploring ferroelectric switching in α-In_2Se_3 for neuromorphic computing. Adv. Funct. Mater. *30*, 2004609. https://doi.org/10.1002/adfm.202004609.

66. Jiang, B., Zou, X., Su, J., Liang, J., Wang, J., Liu, H., Feng, L., Jiang, C., Wang, F., He, J., and Liao, L. (2018). Impact of Thickness on Contact Issues for Pinning Effect in Black Phosphorus Field-Effect Transistors. Adv. Funct. Mater. *28*, 1801398. https://doi.org/10.1002/adfm.201801398.

67. Wells, S.A., Henning, A., Gish, J.T., Sangwan, V.K., Lauhon, L.J., and Hersam, M.C. (2018). Suppressing Ambient Degradation of Exfoliated InSe Nanosheet Devices via Seeded Atomic Layer Deposition Encapsulation. Nano Lett. *18*, 7876–7882. https://doi.org/10.1021/acs.nanolett.8b03689.

68. Chubarov, M., Choudhury, T.H., Hickey, D.R., Bachu, S., Zhang, T., Sebastian, A., Bansal, A., Zhu, H., Trainor, N., Das, S., et al. (2021). Wafer-Scale Epitaxial Growth of Unidirectional WS_2 Monolayers on Sapphire. ACS Nano *15*, 2532–2541. https://doi.org/10.1021/acsnano.0c06750.

69. Zhang, C., Wu, J., Sun, Y., Tan, C., Li, T., Tu, T., Zhang, Y., Liang, Y., Zhou, X., Gao, P., and Peng, H. (2020). High-Mobility Flexible Oxyselenide Thin-Film Transistors Prepared by a Solution-Assisted Method. J. Am. Chem. Soc. *142*, 2726–2731. https://doi.org/10.1021/jacs.9b11668.

70. Li, T., Tu, T., Sun, Y., Fu, H., Yu, J., Xing, L., Wang, Z., Wang, H., Jia, R., Wu, J., et al. (2020). A native oxide high-κ gate dielectric for two-dimensional electronics. Nat. Electron. *3*, 473–478. https://doi.org/10.1038/s41928-020-0444-6.

71. Wang, W., Meng, Y., Wang, W., Zhang, Z., Xie, P., Lai, Z., Bu, X., Li, Y., Liu, C., Yang, Z., et al. (2022). Highly Efficient Full van der Waals 1D p-Te/2D n-Bi_2O_2Se Heterodiodes with Nanoscale Ultra-Photosensitive Channels. Adv. Funct. Mater. *32*, 2203003. https://doi.org/10.1002/adfm.202203003.

72. Wang, W., Meng, Y., Zhang, Y., Zhang, Z., Wang, W., Lai, Z., Xie, P., Li, D., Chen, D., Quan, Q., et al. (2023). Electrically Switchable Polarization in Bi_2O_2Se Ferroelectric Semiconductors. Adv. Mater. *35*, 2210854. https://doi.org/10.1002/adma.202210854.

73. Kresse, G., and Furthmüller, J. (1996). Efficient iterative schemes for ab initio total-energy calculations using a plane-wave basis set. Phys. Rev. B *54*, 11169–11186. https://doi.org/10.1103/PhysRevB.54.11169.

74. Blöchl, P. (1994). Projector augmented-wave method. Phys. Rev. B *50*, 17953–17979. https://doi.org/10.1103/PhysRevB.50.17953.

75. Perdew, J.P., Burke, K., and Ernzerhof, M. (1996). Generalized Gradient Approximation Made Simple. Phys. Rev. Lett. *77*, 3865–3868. https://doi.org/10.1103/PhysRevLett.77.3865.

76. Grimme, S., Antony, J., Ehrlich, S., and Krieg, H. (2010). A consistent and accurate ab initio parametrization of density functional dispersion correction (DFT-D) for the 94 elements H-Pu. J. Chem. Phys. *132*, 154104. https://doi.org/10.1063/1.3382344.